Layer-dependent magnon-magnon coupling in a synthetic antiferromagnet

Yaqi Rong,[1] Chengxin Jiang,[2] Huishan Wang,[2,3] Lu Sun,[1] Fengyu Liu,[1] Juanjuan Lu,[1] Tao Wu,[1] Yu Zhang,[4] Yunshan Zhao,[4] Fusheng Ma,[4,*] Zhiqiang Mu,[2] Haomin Wang,[2] and Yumeng Yang[1,†]

[1] *Shanghai Engineering Research Center of Energy Efficient and Custom AI IC, School of Information Science and Technology, ShanghaiTech University, Shanghai 201210, China*

[2] *State Key Laboratory of Materials for Integrated Circuits, Shanghai Institute of Microsystem and Information Technology, Chinese Academy of Sciences, Shanghai 200050, China*

[3] *Key Laboratory of Optoelectronic Material and Device, Department of Physics, Shanghai Normal University, Shanghai, China*

[4] *Jiangsu Key Laboratory of Opto-Electronic Technology, School of Physics and Technology, Nanjing Normal University, Nanjing 210046, China*

(Received 17 January 2024; revised 26 March 2024; accepted 29 April 2024; published 24 May 2024)

The synthetic antiferromagnet (SAF) offers a versatile platform to couple with various quasiparticles that is an indispensable element for the realization of hybrid quantum computing systems. In this work, we found that the magnon-magnon coupling strength in layered SAFs, consisting of repeated layers of $[Ni_{80}Fe_{20}/Ru]_n$, is highly dependent on the finite layer number n. In particular, the self-hybridizations of individual acoustic or optical modes in the even-layers lead to the opening of local anticrossing gaps within the same type of mode in the resonance spectra. With the structural asymmetry of the odd-layers, a global gap between different modes can be generated whose size is found to decrease with increasing layer number. By combining the static linear chain model with the dynamically coupled Landau-Lifshitz equations, we further formulated a theoretical approach to qualitatively describe such highly layer-dependent behaviors of magnon-magnon coupling in SAFs. It is clear that the layer number is a significant factor that influences both the number of excited modes and the associated mode hybridizations. Our findings shed light on the magnon-magnon coupling in layered antiferromagnets that may invigorate the development of magnonics.

DOI: 10.1103/PhysRevApplied.21.054050

I. INTRODUCTION

The advance of hybrid quantum computing systems [1–4] relies on the coherent transfer and storage of information among a variety of dynamic systems. Among the different information carriers, magnons, or the quanta of spin waves, are of particular interest since they provide a versatile interaction with other quasiparticles, including photons [5,6], phonons [7], spins [8], etc. On-chip magnon-photon and magnon-phonon coupled quantum devices have been demonstrated by employing superconducting resonators [9–11] and surface or bulk acoustic waves [12,13]. Recently, magnon-magnon coupling in magnetic layered structures, arising from the inherent exchange coupling, has attracted increasing attention for its advantage of reaching the strong and ultrastrong coupling regimes as compared with other magnon-mediated hybrid systems [14–17].

The antiferromagnet is an ideal platform with distinct acoustic and optical resonance modes in which to introduce magnon-magnon coupling in the frequency range from tens of gigahertz to a few terahertz. To make these modes more technically accessible, synthetic antiferromagnets (SAFs) [14,18,19] or two-dimensional (2D) layered van der Waals (vdW) magnets [20,21] are more appealing as their magnetizations oscillate in the gigahertz range. The former typically consist of two ferromagnets separated by a nonmagnetic spacer and coupled with a Ruderman-Kittel-Kasuya-Yosida interaction [22]. The latter are cleavable vdW materials with strong intralayer ferromagnetic (FM) coupling but weak interlayer antiferromagnetic (AFM) coupling [20,23]. It has been demonstrated that the coupling between magnon modes can be readily achieved by breaking the rotational symmetry, i.e., the application of an out-of-plane tilted external magnetic field [14,20,24,25], the adoption of different ferromagnets or the same ferromagnets with different thicknesses [26–29], the inclusion of additional magnetocrystalline anisotropy [21,30–32], and the utilization of spin-current-mediated spin pumping and spin

*Corresponding author: phymafs@njnu.edu.cn
†Corresponding author: yangym1@shanghaitech.edu.cn

torques [33–35]. Besides the hybridization of uniform magnon procession, it has been demonstrated that the magnon-magnon coupling strength can be tuned by the angle between the magnetic field and the magnon propagation direction in micro-sized devices with a nonzero wave number [19,36]. More interestingly, the mutual spin pumping between adjacent ferromagnets could lead to dynamic damping modulation that also provides a fertile playground for magnon-based non-Hermitian physics [37,38]. Magnon spin current and magnon torque have also been experimentally excited in magnetic insulators that are related to nonlinear magnon-magnon coupling [34,35,39,40]. When there are more than two FM layers, it is noticed that the SAFs or vdW magnets are still often approximated as a bilayer system with two antiferromagnetically coupled ferromagnets. On the other hand, layer-number-dependent static magnetotransport behaviors have already been reported to cause a drastic modulation of the optoelectronic properties in vdW magnets [41,42]. It is expected that the study on layer-dependent spin dynamics in SAFs or vdW magnets would enrich the understanding of the magnon-magnon coupling in AFM systems, which has rarely been conducted.

In this regard, we theoretically and experimentally studied the magnon-magnon coupling of SAFs with various ferromagnet layer numbers, i.e., $[\mathrm{Py/Ru}]_n$ with n varying from 2 to 7, where Py is used as the abbreviation for $Ni_{80}Fe_{20}$ hereafter. For odd-layer SAFs with structural asymmetry, it is found that a global anticrossing gap is opened, which gradually vanishes with increasing n in accordance with the reduction of asymmetry. Moreover, the self-hybridizations of acoustic-acoustic modes (or optical-optical modes) in the case of even-layer SAFs give rise to individual mode anticrossing gaps within the individual acoustic (or optical) branches. The experimentally observed dependence of magnon-magnon coupling on layer number n of the SAF is in qualitative agreement with the theoretical approach we developed by incorporating both the linear chain model and the n-coupled Landau-Lifshitz (LL) equations. It is evident that in a finite-layer SAF, the layer number n has a major role in determining the number of excited modes as well as the corresponding mode hybridizations. Our results reveal the layer-dependent spin dynamic behaviors in layered magnetic materials, and may stimulate future development of magnonics.

II. SAMPLE PREPARATION AND CHARACTERIZATION METHOD

As illustrated in Fig. 1(a), n-layer SAFs ($n = 2$–7) with a structure of Ta(5 nm)/[Py(3.1 nm)/Ru(1 nm)]$_n$/Ru(2 nm) were prepared on Si/SiO_2 substrates using a magnetron sputtering apparatus (ULVAC, Inc.) at a base pressure of 4×10^{-6} Pa and an Ar working pressure of 0.7 Pa. During the deposition, an *in situ* magnetic field of about 500 Oe was applied to induce the in-plane easy axis (EA) in the x axis. The thickness of the intermediate Ru spacer was tuned to provide AFM interlayer exchange coupling between the adjacent Py layers [22,29]. The bottom Ta was used as a seed layer to promote the structural texture, whereas the top Ru layer was used as a capping layer to inhibit oxidization. All the samples were cut into small pieces of around 0.5×0.5 mm^2 to facilitate the subsequent measurements at room temperature. The static magnetization hysteresis (M-H) loops were firstly obtained by using a vibrating sample magnetometer from Quantum Design with an external magnetic field H applied along x axis. After that, the samples were placed on a coplanar waveguide for dynamic ferromagnetic resonance (FMR) measurements using modules from NanOsc with a dc magnetic field swept in the range of 0–1000 Oe and frequencies varied in the range of 2–8 GHz. Owing to the constraints of the measurement setup, the field direction was fixed in the film plane. To improve signal-to-noise ratio, the transmitted power was converted to a dc voltage by a broadband rf diode, and further measured by the lock-in detection technique with additional ac field modulation at a frequency of 490 Hz. Note that we have chosen the measurement geometry as schematically shown in Fig. 1(a), since both acoustic mode (AM) and optical mode (OM) resonances can be excited when the microwave magnetic field (h_{rf}) has both parallel and perpendicular components with respect to H [43].

III. LAYER-DEPENDENT STATIC MAGNETIC PROPERTIES OF SAF SYSTEMS

Figures 1(b) and 1(c) show the typical M-H loops for the samples with even ($n = 2$, 4, 6) and odd ($n = 3$, 5, 7) layer numbers, respectively. For even-layer SAFs, the loops exhibit a plateau with an almost zero net moment at small field, which indicates the AFM region. The antiparallel alignment of the magnetizations from adjacent Py layers leads to this cancellation of magnetic moment. When H increases above a critical spin-flop (SF) field (H_{SF}), the Zeeman energy overcomes the AFM coupling in the SF region and results in a finite canting of the magnetizations. With a further increase of H to the saturation field (H_{sat}), the magnetizations eventually become parallel to each other in the FM region. It can also be observed that H_{SF} does not change significantly with n and H_{sat} gradually increases with increasing n for the even-layer SAFs. On the other hand, for odd-layer SAFs, the loops show a centering square-shaped hysteresis in the AFM region [see Fig. 1(c)], resembling the behavior of a ferromagnet. This is due to the uncompensated moment in the presence of structural asymmetry with an odd n, and the asymmetry decreases when n increases as manifested by the lowered hysteresis amplitude. Similar to the even-layer case, the

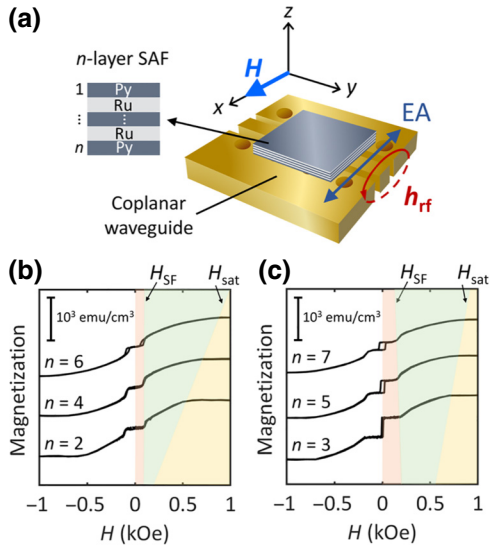

FIG. 1. (a) Schematics of the n-layer synthetic antiferromagnet (SAF) sample placed on the coplanar waveguide with n indicating the number of coupled Py layers. The static external magnetic field H is applied along the easy axis (EA) in the x direction, and the microwave field $h_{\rm rf}$ has both parallel and perpendicular components with respect to H in order to simultaneously excite acoustic and optical modes. (b)–(c) M-H loops of even-layer SAFs ($n=2$, 4, 6) and odd-layer SAFs ($n=3$, 5, 7). The shaded areas highlight the layer-dependent antiferromagnetic (AFM), spin-flop (SF), and ferromagnetic (FM) regions with the critical SF field $H_{\rm SF}$ and saturation field $H_{\rm sat}$.

magnetization of individual ferromagnet layers undergoes the SF and saturation transitions with increasing H. The difference is that $H_{\rm SF}$ here exhibits a descending trend with n, in contrast to the ascending n-dependence of $H_{\rm sat}$.

For a better understanding of the layer-dependent features at finite n values, we invoked a linear chain model to describe the magnetization rotation of the individual ferromagnet layer [41,42]. Under the zero-temperature limit and macrospin approximation where the magnetization of each ferromagnet behaves uniformly, the free-energy density per area of the n-layer SAF system can be expressed as follows:

$$\begin{aligned} E_n(\mathbf{m}_i) &= E_{\rm Zeeman} + E_{\rm dem} + E_k + E_{\rm ex} \\ &= -\mu_0 \mathbf{H} \sum_{i=1}^{n} M_s \mathbf{m}_i + \frac{\mu_0}{2} \sum_{i=1}^{n} (M_s \mathbf{m}_i \cdot \vec{z})^2 \\ &\quad - K_u \sum_{i=1}^{n} (\mathbf{m}_i \cdot \vec{x})^2 + \frac{J}{d} \sum_{i=1}^{n-1} \mathbf{m}_i \cdot \mathbf{m}_{i+1}. \end{aligned} \quad (1)$$

Here, μ_0, M_s, K_u, J, and d are the vacuum permeability, saturation magnetization, in-plane uniaxial anisotropy constant, interlayer exchange coupling constant, and ferromagnet thickness, respectively. $\mathbf{m}_i$ denotes the unit magnetization vector for the ith layer, which can be further written as $\mathbf{m}_i = (\cos\varphi_i, \sin\varphi_i, 0)$; and $\mathbf{H} = (H,\ 0,\ 0)$ implies the applied external field is along the x axis. Accordingly, the first three terms at the right-hand side of Eq. (1) correspond to the Zeeman energy, demagnetization energy, and uniaxial anisotropic energy of $\mathbf{m}_i$; and the fourth term accounts for the exchange coupling energy between the adjacent $\mathbf{m}_i$ and $\mathbf{m}_{i+1}$. Note that ignoring the dipole coupling can be justified since its strength is considerably weaker than the exchange coupling [44, 45]. For convenience, we introduced the expression $H_k = 2K_u/(\mu_0 M_s)$ and $H_{\rm ex} = J/(\mu_0 M_s d)$. The equilibrium state of $\mathbf{m}_i$ (or equivalently φ_i) at a specific H can be numerically determined through energy minimization of Eq. (2) after substituting the vector form of $\mathbf{m}_i$ and $\mathbf{H}$ [42],

$$\begin{aligned} \frac{E(\varphi_i)}{\mu_0 M_s} &= -H \sum_{i=1}^{n} \cos\varphi_i - \frac{H_k}{2} \sum_{i=1}^{n} (\cos\varphi_i)^2 \\ &\quad + H_{\rm ex} \sum_{i=1}^{n-1} \cos(\varphi_i - \varphi_{i+1}). \end{aligned} \quad (2)$$

The calculated static field evolutions of $\mathbf{m}_i$ are plotted in Figs. 2(a)–2(c) ($n=2$, 4, 6) and Figs. 2(d)–2(f) ($n=3$, 5, 7), respectively. The magnetic parameters of the SAFs used in the numerical calculations are extracted from Figs. 1(b) and 1(c) and further summarized in Table I. In accordance with the description of Fig. 2, three distinct regions are clearly identified from the φ_i versus H curves along with the increase of H: (i) AFM region with $\varphi_i = 0$ and $\varphi_{i+1} = \pi$; (ii) SF region with φ_i and φ_{i+1} near $\pm\pi/2$; and (iii) FM region with $\varphi_i = 0$ and $\varphi_{i+1} = 0$. We can also identify from Fig. 2 that $\mathbf{m}_i$ and $\mathbf{m}_{n+1-i}$ tend to form a pair that respond together to H. However, the detailed evolution of $\mathbf{m}_i$ exhibits a noticeable difference for even- and odd-layer SAFs in the studied range of $n=2$–7, which is illustrated in Figs. 2(g) and 2(h) by using $n=3$ and 4 as examples with the arrows qualitatively indicating the individual layer rotation. For even-layer SAFs [see Figs. 2(a)–2(c)], with all Py layers successfully forming a total of $n/2$ pairs, a fully compensated SAF structure is obtained since the paired $\mathbf{m}_i$ and $\mathbf{m}_{n+1-i}$ always behave symmetrically with respect to H. This gives rise to the almost zero moment in the AFM region as observed in Fig. 1(b). Moreover, $\mathbf{m}_i$ and $\mathbf{m}_{n+1-i}$ would suddenly flop from the antiparallel state aligned along the x axis to the flopped state near the y axis, and then gradually rotate toward the x axis again in a symmetrical way. On the other hand, in the case of odd-layer SAFs, there is always an unpaired $\mathbf{m}_{(n+1)/2}$ so that a finite magnetic moment is observed even in the AFM region [see Fig. 1(c)]. In the presence of such asymmetry, $\mathbf{m}_i$ and $\mathbf{m}_{n+1-i}$ would rather

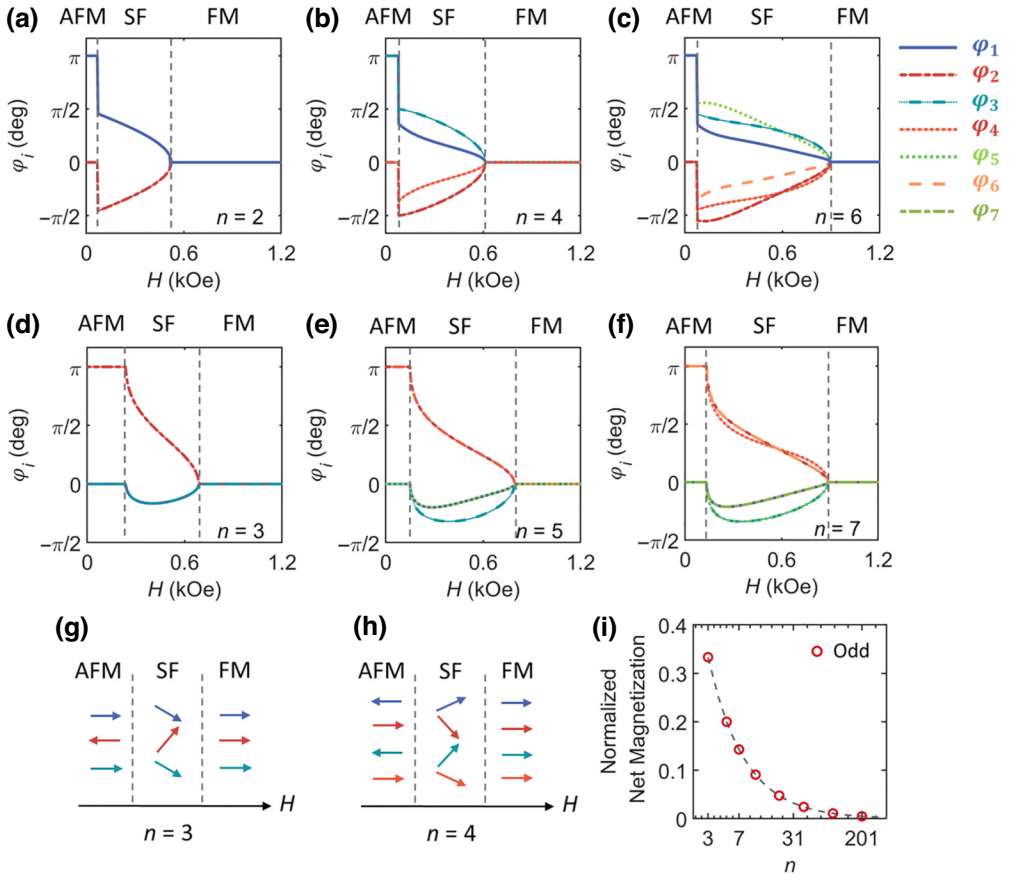

FIG. 2. Numerically calculated magnetization evolution of each layer in SAFs using the static linear chain model as Eq. (2) in the presence of H with (a)–(c) even-layer SAFs ($n = 2$, 4, 6) and (d)–(f) odd-layer SAFs ($n = 3$, 5, 7), where φ_i represents the angle between the magnetization of the ith layer with respect to H. Taking $n = 3$ and 4 as examples, the arrows in (g),(h) are used to qualitatively illustrate the direction of $\mathbf{m}_i$ during field sweeping. (i) Calculated net magnetization as a function of n for odd-layer SAFs.

respond to H in the same manner, and undergo a gradual transition to the flopped position before finally entering the FM region. These subtle differences in the static position of φ_i with finitely small n would make the dynamic coupling between different magnon modes possible, which will be discussed in the next section.

More quantitatively, we also analyzed the layer dependence of H_{SF} and H_{sat} from Eq. (2). At $H = H_{SF}$ when $\mathbf{m}_i$ gets canted, there is a solution of φ_i near $\pm\pi/2$, in addition to the antiparallel solution of 0 and π. Equivalently, by treating H as a variable and numerically solving the following Eq. (3) at around $\varphi_i = \pm\pi/2$, we could determine the critical value of H_{SF} [42].

$$
\begin{aligned}
E(\varphi_1, \varphi_2, \ldots) &= E(0, \pi, \ldots) \\
&\quad - H \sum_{i=1}^{n} \cos\varphi_i - \frac{H_k}{2} \sum_{i=1}^{n} (\cos\varphi_i)^2 \\
&\quad + H_{ex} \sum_{i=1}^{n-1} \cos(\varphi_i - \varphi_{i+1}) \\
&= \begin{cases} -\dfrac{n}{2} H_k + (n-1) H_{ex} & \text{for even } n \\ -\dfrac{n}{2} H_k + (n-1) H_{ex} + H & \text{for odd } n \end{cases}
\end{aligned}
\tag{3}
$$

As can be inferred, in the case of even-layer SAFs, H_{SF} is weakly dependent on n as it does not contain any H-related term on the right-hand side. The situation becomes different with the appearance of H from the structural asymmetry in the odd-layer case. With an increase in n, the contribution of H in Eq. (3) keeps decreasing before getting negligibly small with the reduction of asymmetry, which results in the descending trend of H_{SF} with n. In addition, when $\mathbf{m}_i$ becomes fully aligned with H (i.e., $\varphi_i = 0$) at $H = H_{sat}$, H_{sat} would keep increasing with n as it results from the overcoming of E_{ex} by E_{Zeeman}. Another interesting point to note is that when n finally becomes very

TABLE I. A summary of the magnetic parameters extracted from M-H loops of n-layer SAFs that are used for numerical calculations.

n	M_s (emu cm^{-3})	H_{ex} (Oe)	H_k (Oe)	H_{SF} (Oe)	H_{sat} (Oe)
2	571	267	10	72	523
3	789	230	3	236	688
4	693	185	18	82	614
5	766	220	3	149	792
6	722	243	12	77	898
7	656	235	5	132	888

large, the n-layer SAF can always be approximated as a bilayer system with two magnetization sublattices regardless of having an even or odd n, since the term containing H would contribute a vanishingly small amount to the total energy in Eq. (3). This is further supported by the reduction of net magnetization as a function of n in odd-layer SAFs that is calculated in Fig. 2(i). In other words, the layer-dependent M-H loops of SAFs are only observed with a finitely small n so that the top and bottom surface boundaries play a role in the magnetic properties.

IV. LAYER-DEPENDENT SPIN DYNAMICS OF SAF SYSTEMS

Before discussing experimental results, we describe how we modeled the dynamic characteristics of an n-layer SAF by employing the n-coupled LL equations. Considering the low damping and small in-plane anisotropy of Py (see Table I), these terms are omitted for simplicity. The dynamics of the SAF system is described where the surface layers ($i=1$ and n) and the internal layer ($i=2$ to $n-1$) are described separately as follows:

$$\begin{cases} \frac{d\mathbf{m}_1}{dt} = -\mu_0\gamma\mathbf{m}_1 \times [H\vec{x} - H_{\mathrm{ex}}\mathbf{m}_2 - M_s(\mathbf{m}_1\cdot\vec{z})\vec{z}], & i=1, \\ \frac{d\mathbf{m}_i}{dt} = -\mu_0\gamma\mathbf{m}_i \times [H\vec{x} - H_{\mathrm{ex}}\mathbf{m}_{i-1} - H_{\mathrm{ex}}\mathbf{m}_{i+1} - M_s(\mathbf{m}_i\cdot\vec{z})\vec{z}], & i=2,\ldots,n-1, \\ \frac{d\mathbf{m}_n}{dt} = -\mu_0\gamma\mathbf{m}_n \times [H\vec{x} - H_{\mathrm{ex}}\mathbf{m}_{n-1} - M_s(\mathbf{m}_n\cdot\vec{z})\vec{z}], & i=n. \end{cases} \tag{4}$$

Here, γ is the gyromagnetic ratio and t is the time. To facilitate the derivation, a new $X_iY_iZ_i$ coordinate system is introduced where X_i is parallel to the static equilibrium direction of $\mathbf{m}_i$. In this way, the time-dependent precession of $\mathbf{m}_i$ at angular frequency ω is written as $\mathbf{m}_i(t) = (1, \tilde{m}_i^Y e^{j\omega t}, \tilde{m}_i^Z e^{j\omega t})$ with $\tilde{m}_i^Y$ and $\tilde{m}_i^Z$ describing the dynamic precession amplitude in the $X_iY_iZ_i$ system. The coordinate transformation is subsequently performed on Eq. (4) by rotating the original xyz system with the angle φ_i, in which φ_i is obtained from numerically solving the static linear chain model of Eq. (2) as shown in Fig. 2. For convenience, φ_i is taken as the absolute value of the angle between $\mathbf{m}_i$ and H in the following derivation. On this basis, Eq. (4) can be linearized in the $X_iY_iZ_i$ coordinate with respect to $\tilde{m}_i^Y$ and $\tilde{m}_i^Z$ with $i=1,2,\ldots,n$. The as-obtained matrix equation is thus given by

$$j\omega \begin{pmatrix} \tilde{m}_1^Y \\ \tilde{m}_1^Z \\ \tilde{m}_2^Y \\ \tilde{m}_2^Z \\ \vdots \\ \tilde{m}_i^Y \\ \tilde{m}_i^Z \\ \vdots \\ \tilde{m}_{n-1}^Z \\ \tilde{m}_n^Y \\ \tilde{m}_n^Z \end{pmatrix} + \mu_0\gamma \begin{pmatrix} 0 & H_{\mathrm{eq},1}+M_s & 0 & H_{\mathrm{ex}} & & & & & & & \\ -H_{\mathrm{eq},1} & 0 & -H_{\mathrm{ex},1} & 0 & 0 & & & & & & \\ 0 & H_{\mathrm{ex}} & 0 & H_{\mathrm{eq},2}+M_s & 0 & H_{\mathrm{ex}} & & & & & \\ -H_{\mathrm{ex},1} & 0 & -H_{\mathrm{eq},2} & 0 & -H_{\mathrm{ex},2} & 0 & 0 & & & & \\ & \ddots & \ddots & \ddots & \ddots & \ddots & \ddots & \ddots & & & \\ & & 0 & 0 & H_{\mathrm{ex}} & 0 & H_{\mathrm{eq},i}+M_s & 0 & H_{\mathrm{ex}} & & \\ & & & -H_{\mathrm{ex},i-1} & 0 & -H_{\mathrm{eq},i} & 0 & -H_{\mathrm{ex},i} & 0 & 0 & \\ & & & & \ddots & \ddots & \ddots & \ddots & \ddots & \ddots & \ddots \\ & & & & & -H_{\mathrm{ex},n-2} & 0 & -H_{\mathrm{eq},n-1} & 0 & -H_{\mathrm{ex},n-1} & 0 \\ & & & & & & 0 & 0 & H_{\mathrm{ex}} & 0 & H_{\mathrm{eq},n}+M_s \\ & & & & & & & -H_{\mathrm{ex},n-1} & 0 & -H_{\mathrm{eq},n} & 0 \end{pmatrix} \begin{pmatrix} \tilde{m}_1^Y \\ \tilde{m}_1^Z \\ \tilde{m}_2^Y \\ \tilde{m}_2^Z \\ \vdots \\ \tilde{m}_i^Y \\ \tilde{m}_i^Z \\ \vdots \\ \tilde{m}_{n-1}^Z \\ \tilde{m}_n^Y \\ \tilde{m}_n^Z \end{pmatrix} = 0, \tag{5}$$

where $H_{\mathrm{ex},i} = H_{\mathrm{ex}}\cos(\varphi_i + \varphi_{i+1})$ represents the effective exchange coupling field between the ith and $(i+1)$-th layers along the X_i direction, and $H_{\mathrm{eq},i}$ is the total effective field along X_i direction in the form of

$$H_{\mathrm{eq},i} = \begin{cases} H\cos\varphi_1 - H_{\mathrm{ex},1}, & i=1 \\ H\cos\varphi_i - H_{\mathrm{ex},i-1} - H_{\mathrm{ex},i}, & i=2,\ \cdots,\ n-1 \\ H\cos\varphi_n - H_{\mathrm{ex},n-1}, & i=n \end{cases}. \tag{6}$$

Equation (5) represents a typical matrix eigenvalue problem with $[\mathbf{H}]\{\mathbf{m}\} = \omega\{\mathbf{m}\}$, where $\{\mathbf{m}\}$ is the column vector consisting of the individual magnetization precession amplitudes and the $[\mathbf{H}]$ matrix contains the effective field elements multiplied by $\mu_0\gamma j$. The resonant frequencies $f = \omega/(2\pi)$ of n-layer SAFs are obtained as the eigenvalues of the $[\mathbf{H}]$ matrix, which are real numbers for a Hermitian matrix without the consideration of damping terms. Furthermore, for even-layer SAFs with a symmetric structure, by substituting $\tilde{m}_{n/2}^{Y(Z)} = \pm\tilde{m}_{(n/2)+1}^{Y(Z)}$ into half of the $n/2$ coupled LL equations, we could solve acoustic

and optical eigenvalues separately using a reduced n-order [**H**] matrix with + and − following the aforementioned notion for AM and OM frequencies, respectively [46]. However, for the odd-layer case, the entire n-coupled LL equations and the associated $2n$-order [**H**] matrix have to be considered due to the broken structural symmetry. It should be noted that the [**H**] matrix would become non-Hermitian with the inclusion of the damping terms in Eq. (4). The mutual spin pumping from adjacent Py layers would further induce a layer-dependent modification of damping. Such differences in damping for different Py layers could eventually break the structural symmetry that affects the magnon-magnon coupling strength [33,46]. While little information is known about the spin-current transport parameters in different layers, we choose to have a more general understanding of the Hermitian [**H**] matrix by neglecting all the damping-related terms.

We can anticipate from Eq. (5) that the first and nth layer at the surfaces only have one effective exchange field with the adjacent second and $(n-1)$-th layer. This in fact is the cause for the n-dependent spin dynamics at finitely small n. When n increases to a very large value, it can be approximated by periodic boundary conditions on the first and nth layer so that each layer of the SAF can be considered as $\mathbf{m}_i$ with two adjacent layers $\mathbf{m}_{i-1}$ and $\mathbf{m}_{i+1}$. In this sense, we could use one generalized LL equation to represent the n-layer system.

$$\frac{d\mathbf{m}_i}{dt} = -\mu_0\gamma\mathbf{m}_i \times [H\vec{x} - H_{\rm ex}\mathbf{m}_{i-1} - H_{\rm ex}\mathbf{m}_{i+1} - M_s(\mathbf{m}_i\cdot\vec{z})\vec{z}], \quad i = 1,\ldots,n. \tag{7}$$

As inferred from the field evolution of φ_i in Fig. 2, we could further approximate the adjacent $\mathbf{m}_{i-1}$ and $\mathbf{m}_{i+1}$ as behaving in the same way, so that the $\mathbf{m}_{i+1}$ terms can be combined with the $\mathbf{m}_{i-1}$ terms during linearization. The linearized matrix equation in the new $X_iY_iZ_i$ coordinate is thus given by

$$j\omega\begin{pmatrix}\tilde{m}^Y_{i-1}\\ \tilde{m}^Z_{i-1}\\ \tilde{m}^Y_i\\ \tilde{m}^Z_i\end{pmatrix} + \mu_0\gamma \times \begin{pmatrix} 0 & H_{\rm eq}+M_s & 0 & 2H_{\rm ex}\\ -H_{\rm eq} & 0 & -2H_{{\rm ex},i} & 0\\ 0 & 2H_{\rm ex} & 0 & H_{\rm eq}+M_s\\ -2H_{{\rm ex},i} & 0 & -H_{\rm eq} & 0\end{pmatrix} \times \begin{pmatrix}\tilde{m}^Y_{i-1}\\ \tilde{m}^Z_{i-1}\\ \tilde{m}^Y_i\\ \tilde{m}^Z_i\end{pmatrix} = 0. \tag{8}$$

Here, $H_{{\rm ex},i} = H_{\rm ex}\cos(2\varphi_i)$ and $H_{\rm eq} = H\cos\varphi_i - 2H_{{\rm ex},i}$, with the additional requirement of $|\varphi_{i-1}| = |\varphi_i|$ due to the symmetric structure. The four-order matrix [**H**] in Eq. (8) is similar to that of the bilayer SAF that gives the resonance frequency of AM (+) and OM (−) as [47]

$$\left(\frac{2\pi f_{+(-)}}{\gamma\mu_0}\right)^2 = \frac{H^2}{2} + 2M_sH_{\rm ex} \pm \left(\frac{H^2}{2} + \frac{M_sH^2}{4H_{\rm ex}} - 2M_sH_{\rm ex}\right). \tag{9}$$

This explains why the FMR spectra of 2D vdW magnets agree with the results derived from the bilayer system even with many ferromagnetic layers [20].

Outside the SF region, the resonance characteristics for the AFM and FM regions can also be obtained by linearizing Eq. (4) with the inclusion of H_k [18,47,48]. As an example, the spin dynamics of a typical bilayer SAF are first depicted in Fig. 3(a). In the AFM region, the two magnetizations are initially aligned to be antiparallel and start to precess around the x axis in phase (or out of phase). Note that it is usually difficult to experimentally observe the AM since the dynamic components of the magnetizations tend to cancel out [49]. In the SF region, both magnetizations precess around the flopped equilibrium positions near the y axis following the AM or OM resonance as illustrated in Fig. 3(d). Here, the resonance frequencies of the AM and OM intersect at the crossing point of $(H_{\rm cross}, f_{\rm cross})$. As discussed previously [20,28], the magnon-magnon coupling, referring to the hybridization of the AM and OM, could open an anticrossing gap at $H_{\rm cross}$ that causes the splitting of the resonance frequency. The effective mutual coupling strength g is quantitatively determined as $g/2\pi = \min|(f_+ - f_-)/2|$, where $f_{+(-)}$ refers to the frequency of the AM (OM). In the FM region where the magnetizations are both parallel to H, the in-phase AM is enhanced while the out-of-phase OM vanishes in the experiment. Figures 3(b) and 3(c) further plot the calculated resonance characteristics for $n = 3$ and $n = 4$ as typical examples for the odd- and even-layers at an increased layer number. Similarly, the global magnetization precessions of individual Py layers are illustrated in Figs. 3(e) and 3(f) for AM and OM resonance in the SF region. Note that the precession trajectory can be obtained by substituting the eigenvectors of the [**H**] matrix into $\mathbf{m}_i(t)$ (see Supplemental Material for magnetization precession trajectory in different modes [50]). The layer-dependent difference in precession would lead to an increase in the number of modes, which will be discussed in the following.

After clarifying the bilayer SAF as a basis, Figs. 4(a) and 4(b) show the measured derivative of transmitted

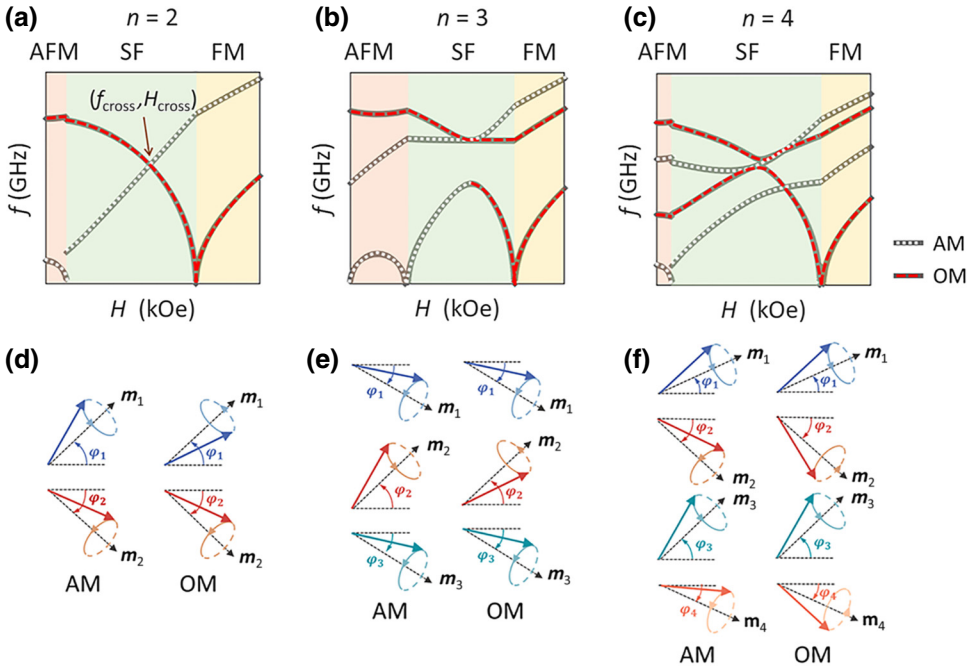

FIG. 3. Illustration of the acoustic mode (AM; dotted line) and optical mode (OM; dashed line) characteristic frequencies of SAFs with (a) $n=2$, (b) $n=3$, (c) $n=4$ obtained from the numerical calculation of Eq. (4), which can be divided into the AFM, SF, and FM regions based on the static equilibrium state of the magnetizations. Illustrated magnetization precessions for acoustic and optical modes in the SF region for (d) $n=2$, (e) $n=3$, (f) $n=4$.

microwave power (dP/dH) as a function of H at low-frequency and high-frequency regions for even- and odd-layer SAFs as typical examples. In general, the global OM and AM resonances, similar to bilayer ($n=2$) in Fig. 3(a), are observed when n is increased to 3–7, which is labeled as "OM_g" and "AM_g" in Figs. 4(a) and 4(b), while their resonance intensity gradually weakens with increasing n. Here, the global AM (or OM) resonance refers to the in-phase (or out-of-phase) precession between any pair of two adjacent magnetizations, as shown in Figs. 3(d)–3(f). For the low-frequency region, the main AM_g (and OM_g) always appears at small (and large) fields with the appearance of an additional local mode OM_l at small field once $n=5$–7. In contrast to the global mode, not all the pairs formed by adjacent magnetizations precess in an in-phase (or out-of-phase) manner, so that this type of precession is collectively labeled as AM_l (or OM_l) (See Supplemental Material [50] Sec. I for details). Furthermore, the resonance intensity of OM_g for even-layer SAFs tends to be greater than that of AM_g, and such differences between the two gradually reduce with the increase of n [left panel of Fig. 4(a)]. In contrast, the AM_g intensity is initially higher than OM_g for odd-layer SAFs at $n=3$, and it eventually becomes weaker than OM_g as n increases to 7 [right panel of Fig. 4(a)]. For the high-frequency region, the situation becomes complicated due to the additional appearance of more resonance branches and the hybridization between different magnon modes. According to Fig. 3(a), the AM_g (and OM_g) should appear at large (and small) fields so that a crossing point is observed at (H_{cross}, f_{cross}). This is indeed observed for $n=2$–5, except that an additional OM_l is generated with $n=4$ and 5 in the large field due to hybridization. For the remaining cases ($n=6$ and 7), another AM_l is generated at the large field in addition to the OM_l for $n=6$, and only an AM_g is observed with the presence of the additional OM_l for $n=7$. Moreover, despite the decrease of intensity for the OM_g with the increase of n, AM_g maintains a relatively strong resonance intensity.

To have a better view of the magnon-magnon coupling, we further present more detailed experimental resonance phase diagrams as functions of both frequency and field in Figs. 5(a)–5(c) for even-layer SAFs with $n=2$, 4, 6 and Figs. 5(g)–5(i) for odd-layer SAFs with $n=3$, 5, 7, respectively (see Supplemental Material for unguided experimental resonance spectra [50]). Through numerically solving Eq. (5) with different n values, the calculated resonance frequency curves as a function of field are plotted in Figs. 5(d)–5(f) for even-layer SAFs with $n=2$, 4, 6 (solid lines) and Figs. 5(j)–5(l) for odd-layer SAFs with $n=3$, 5, 7 (solid lines), respectively. Note that the dashed and dotted lines are added in the figures to serve as guides to distinguish OM and AM resonances. For $n=2$, as

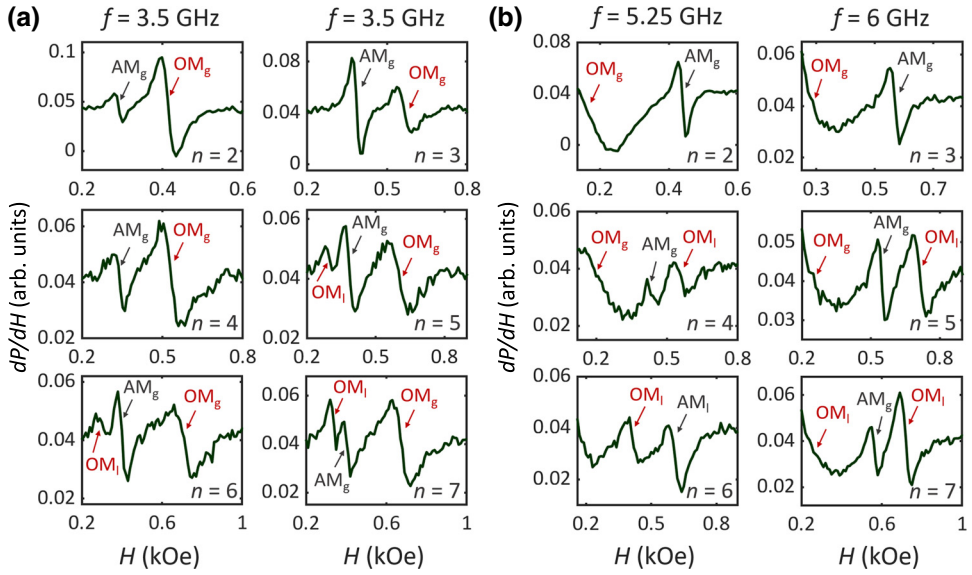

FIG. 4. The measured derivative of transmitted microwave power dP/dH as a function of the magnetic field for n-layer SAFs at (a) low-frequency ($f = 3.5$ GHz for both even and odd layers) region, and (b) high-frequency ($f = 5.25$ GHz for even layers and $f = 6$ GHz for odd layers) region.

shown in Figs. 5(a) and 5(d), without any mode hybridization in the symmetric measurement configuration [20], the two modes appear "crossed" at 0.35 kOe. When n increases to 4 and 6, additional high-frequency (or low-frequency) branches start to appear as AMs (or OMs) with the branch number of the AM (or OM) determined by $n/2$. More interestingly, a separate gap can be observed when looking at the AM or OM branches alone. As shown in Fig. 2, with a finite even n in the case of symmetric structures, the magnetization of individual ferromagnets flops to slightly different positions near $\pm\pi/2$ in the SF region. Such a difference in the static position gives rise to the difference in resonances of individual ferromagnets that allows the self-hybridization of magnon modes. In particular, the anticrossing gaps observed near 0.4 kOe in Figs. 5(b) and 5(e) for $n = 4$ can be considered as the splitting of the original single branch for $n = 2$ into two, which is attributed to the additional low-frequency (high-frequency) excitation of the OM (AM) on the surface layer (in the interior layer) [46]. Although the resonance spectra of $n = 6$ is even more complicated with the further splitting into three branches of OMs (or AMs) [see Figs. 5(c) and 5(f)], a similar self-hybridization situation occurs as manifested by the opening of an anticrossing gap near 0.6 kOe. On the other hand, the odd-layer SAFs always have a structural asymmetry due to the unpaired $\mathbf{m}_{(n+1)/2}$ layer that provides a dynamically changing H_{ex} to its adjacent layers during procession. As a result, the FMR spectra of $n = 3$ and 5 can be viewed as the mode-splitting cases from $n = 2$ with the appearance of a global anticrossing gap near 0.5 kOe and 0.45 kOe, respectively [see Figs. 5(g), 5(h), 5(j), 5(k)]. Similar to the even-layer case, the mode splits into n branches due to the differences in resonance of different ferromagnet layers. The appearance of additional resonance branches in turn squeezes the gap, in accordance to the decreased structural asymmetry and magnon-magnon coupling with the increase of n [see Figs. 5(i) and 5(l)]. It is now experimentally clear that the layer number n is a significant factor that influences both the number of excited modes and the associated mode hybridizations in a finite-layer SAF.

We quantitatively discuss the coupling strength of SAFs using the experimental data extracted from $n = 3$ and 4 as typical examples for the odd- and even-layer cases. It is known that the condition to achieve strong magnon-magnon coupling is $g > \kappa_a, \kappa_o$, where $\kappa_a/2\pi$ (or $\kappa_o/2\pi$) is the dissipation rate for AM (or OM) resonance determined from the half maximum linewidth [51]. For $n = 3$, the extracted effective mutual coupling strength $g/2\pi = 0.556 \pm 0.181$ GHz [black arrow in Fig. 5(a)] is comparable with $\kappa_a/2\pi$, $\kappa_o/2\pi$ in the range of 0.056 to 0.883 GHz, falling into the intermediate coupling-strength regime. As the intrinsic excitation frequency is $f_r = (f_+ + f_-)/2 = 4.914 \pm 0.336$ GHz, the normalized coupling rate $\eta = g/(2\pi f_r)$ becomes 0.116 ± 0.043 [31,52,53]. Similarly for $n = 4$, we could also estimate the individual AM-AM coupling strength $g_a/2\pi$ as 0.414 ± 0.086 GHz and η_a as 0.075 ± 0.025. In both cases, the magnon-magnon coupling strength approaches the strong-coupling regime, and further exhibits a diminishing trend with increasing n.

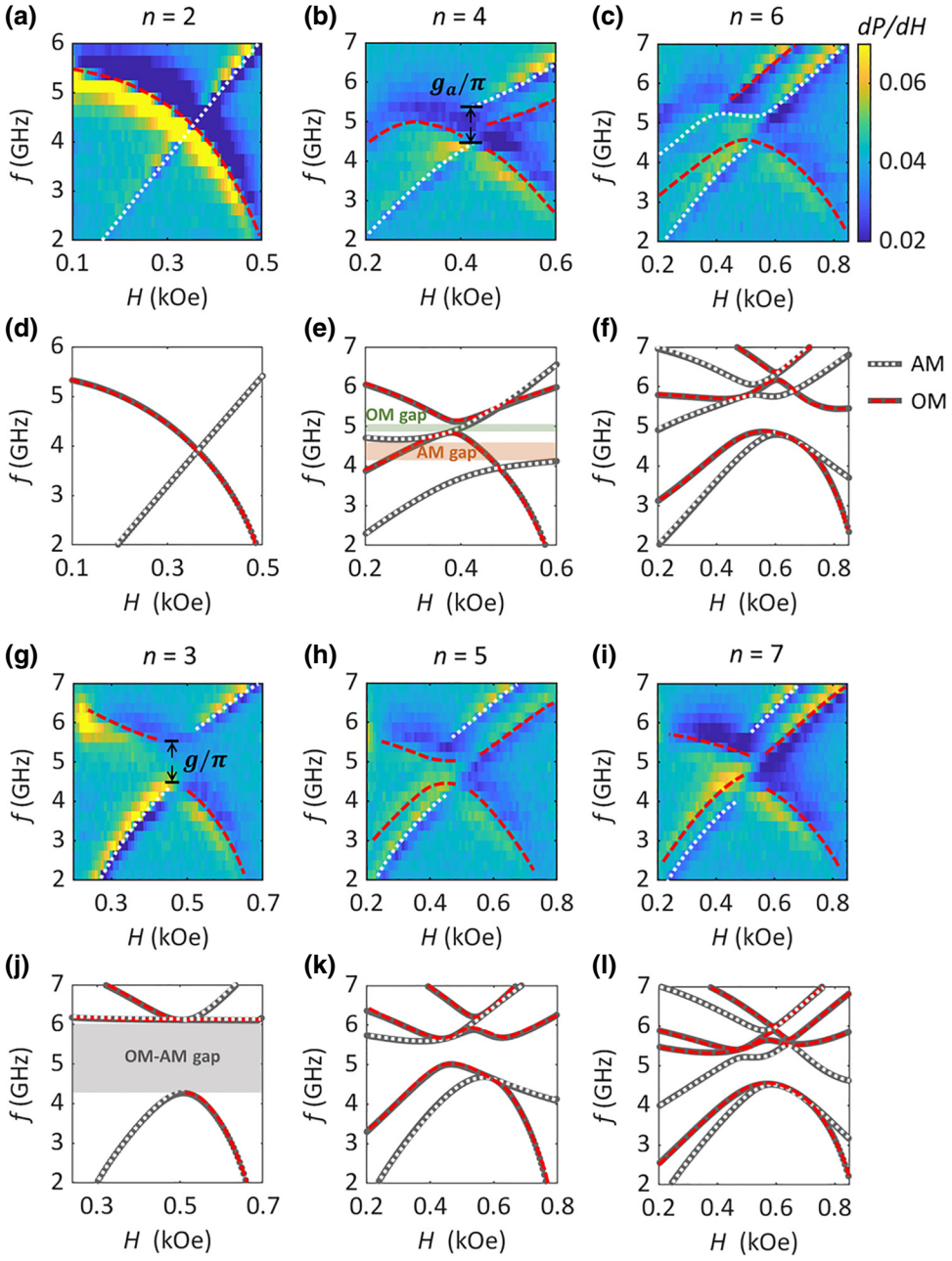

FIG. 5. The measured derivative of transmitted microwave power *dP/dH* as a function of frequency and magnetic field for even-layer SAFs with (a) $n=2$, (b) $n=4$, (c) $n=6$, and odd-layer SAFs with (g) $n=3$, (h) $n=5$, (i) $n=7$. The calculated acoustic mode (AM) and optical mode (OM) characteristic frequencies obtained by numerically solving the coupled LL equations as Eq. (4) with (d) $n=2$, (e) $n=4$, (f) $n=6$, (j) $n=3$, (k) $n=5$, and (l) $n=7$. Note that the dashed lines (or dotted lines) serve as guidance to indicate the OM (or AM) resonance frequency. Unguided figures can be found in the Supplementary Material Sec. II. The arrow in (b) indicates $(f_+ - f_-) = g_a/\pi$, which is twice the AM-AM coupling strength. The shaded areas in (e) serve as guidance for the individual acoustic or optical gap induced by self-hybridization. The arrow in (g) indicates $(f_+ - f_-) = g/\pi$, which is twice the OM-AM coupling strength. The shaded areas in (j) serve as guidance for the global OM-AM gap through hybridization.

V. CONCLUSION

In summary, we have experimentally demonstrated that magnon-magnon coupling is highly dependent on the number of ferromagnet layers in SAFs. In particular, the odd-layer SAFs have sizable anticrossing gaps due to the presence of structural asymmetry, while the self-hybridizations of acoustic or optical modes in even-layer SAFs lead to the opening of gaps within the same type of modes. On this basis, we combined the static linear

chain model and the dynamically n-coupled LL equations to account for the layer-dependent resonance spectra, and found a qualitative consistency between the experimental and numerical results. It was discovered that the number of layers n has a significant impact on both the number of excitation modes and the mode hybridizations in finite-layer SAFs. We envision that our findings could be transferable to other layered SAFs and 2D vdW magnets and provide more possibilities for the development of magnonics.

ACKNOWLEDGMENTS

This work was supported by the National Key Research and Development Program of China (Grants No. 2022YFB4401700, No. 2022YFF0609800), the National Natural Science Foundation of China (Grants No. 62074099, No. 12074189), the Open Research Fund of State Key Laboratory of Materials for Integrated Circuits (Grant No. NKLJC-K2023-02), the ShanghaiTech Quantum Device Lab and Platform of Mechatronics, Energy, and Electronic Devices.

[1] Y. Li, W. Zhang, V. Tyberkevych, W.-K. Kwok, A. Hoffmann, and V. Novosad, Hybrid magnonics: Physics, circuits, and applications for coherent information processing, J. Appl. Phys. **128**, 130902 (2020).

[2] H. Y. Yuan, Y. Cao, A. Kamra, R. A. Duine, and P. Yan, Quantum magnonics: When magnon spintronics meets quantum information science, Phys. Rep. **965**, 1 (2022).

[3] D. D. Awschalom, C. R. Du, R. He, F. J. Heremans, A. Hoffmann, J. Hou, H. Kurebayashi, Y. Li, L. Liu, V. Novosad, *et al.*, Quantum engineering with hybrid magnonic systems and materials, IEEE Trans. Quantum Eng. **2**, 1 (2021).

[4] A. Barman, G. Gubbiotti, S. Ladak, A. O. Adeyeye, M. Krawczyk, J. Gräfe, C. Adelmann, S. Cotofana, A. Naeemi, V. I. Vasyuchka, *et al.*, The 2021 magnonics roadmap, J. Phys.: Condens. Matter **33**, 413001 (2021).

[5] A. W. Elshaari, W. Pernice, K. Srinivasan, O. Benson, and V. Zwiller, Hybrid integrated quantum photonic circuits, Nat. Photonics **14**, 285 (2020).

[6] Y. Yang, Y. Xiao, and C. M. Hu, Theory of Floquet-driven dissipative cavity magnonics, Phys. Rev. B **107**, 054413 (2023).

[7] R. Anufriev and M. Nomura, in *Quantum Hybrid Electronics and Materials*, edited by Y. Hirayama, K. Hirakawa, H. Yamaguchi (Springer Nature Singapore, Singapore, 2022), pp. 15.

[8] P.-B. Li, Y. Zhou, W.-B. Gao, and F. Nori, Enhancing spin-phonon and spin-spin interactions using linear resources in a hybrid quantum system, Phys. Rev. Lett. **125**, 153602 (2020).

[9] H. Huebl, C. W. Zollitsch, J. Lotze, F. Hocke, M. Greifenstein, A. Marx, R. Gross, and S. T. B. Goennenwein, High cooperativity in coupled microwave resonator ferrimagnetic insulator hybrids, Phys. Rev. Lett. **111**, 127003 (2013).

[10] Y. Li, V. G. Yefremenko, M. Lisovenko, C. Trevillian, T. Polakovic, T. W. Cecil, P. S. Barry, J. Pearson, R. Divan, V. Tyberkevych, *et al.*, Coherent coupling of two remote magnonic resonators mediated by superconducting circuits, Phys. Rev. Lett. **128**, 047701 (2022).

[11] Y. Li, T. Polakovic, Y. L. Wang, J. Xu, S. Lendinez, Z. Zhang, J. Ding, T. Khaire, H. Saglam, R. Divan, *et al.*, Strong coupling between magnons and microwave photons in on-chip ferromagnet-superconductor thin-film devices, Phys. Rev. Lett. **123**, 107701 (2019).

[12] S. G. Alekseev, S. E. Dizhur, N. I. Polzikova, V. A. Luzanov, A. O. Raevskiy, A. P. Orlov, V. A. Kotov, and S. A. Nikitov, Magnons parametric pumping in bulk acoustic waves resonator, Appl. Phys. Lett. **117**, 072408 (2020).

[13] K. An, A. N. Litvinenko, R. Kohno, A. A. Fuad, V. V. Naletov, L. Vila, U. Ebels, G. de Loubens, H. Hurdequint, N. Beaulieu, *et al.*, Coherent long-range transfer of angular momentum between magnon Kittel modes by phonons, Phys. Rev. B **101**, 060407 (2020).

[14] A. Sud, C. W. Zollitsch, A. Kamimaki, T. Dion, S. Khan, S. Iihama, S. Mizukami, and H. Kurebayashi, Tunable magnon-magnon coupling in synthetic antiferromagnets, Phys. Rev. B **102**, 100403 (2020).

[15] Y. Xiong, Y. Li, M. Hammami, R. Bidthanapally, J. Sklenar, X. Zhang, H. Qu, G. Srinivasan, J. Pearson, A. Hoffmann, *et al.*, Probing magnon–magnon coupling in exchange coupled $Y_3Fe_5O_{12}$/permalloy bilayers with magneto-optical effects, Sci. Rep. **10**, 12548 (2020).

[16] Z. Li, J. Sun, and F. Ma, Floquet engineering of selective magnon–magnon coupling in synthetic antiferromagnets, Appl. Phys. Lett. **123**, 232406 (2023).

[17] J. Chen, C. Liu, T. Liu, Y. Xiao, K. Xia, G. E. W. Bauer, M. Wu, and H. Yu, Strong interlayer magnon-magnon coupling in magnetic metal-insulator hybrid nanostructures, Phys. Rev. Lett. **120**, 217202 (2018).

[18] H. J. Waring, N. A. B. Johansson, I. J. Vera-Marun, and T. Thomson, Zero-field optic mode beyond 20 GHz in a synthetic antiferromagnet, Phys. Rev. Appl. **13**, 034035 (2020).

[19] Y. Shiota, T. Taniguchi, M. Ishibashi, T. Moriyama, and T. Ono, Tunable magnon-magnon coupling mediated by dynamic dipolar interaction in synthetic antiferromagnets, Phys. Rev. Lett. **125**, 017203 (2020).

[20] D. MacNeill, J. T. Hou, D. R. Klein, P. Zhang, P. Jarillo-Herrero, and L. Liu, Gigahertz frequency antiferromagnetic resonance and strong magnon-magnon coupling in the layered crystal $CrCl_3$, Phys. Rev. Lett. **123**, 047204 (2019).

[21] W. Li, Y. Dai, L. Ni, B. Zhang, D. Tang, Y. Yang, and Y. Xu, Ultrastrong magnon–magnon coupling and chirality switching in antiferromagnet $CrPS_4$, Adv. Funct. Mater. **33**, 2303781 (2023).

[22] P. Bruno and C. Chappert, Oscillatory coupling between ferromagnetic layers separated by a nonmagnetic metal spacer, Phys. Rev. Lett. **67**, 1602 (1991).

[23] C. Hu, K. N. Gordon, P. Liu, J. Liu, X. Zhou, P. Hao, D. Narayan, E. Emmanouilidou, H. Sun, Y. Liu, *et al.*, A van der Waals antiferromagnetic topological insulator with weak interlayer magnetic coupling, Nat. Commun. **11**, 97 (2020).

[24] A. H. Comstock, C.-T. Chou, Z. Wang, T. Wang, R. Song, J. Sklenar, A. Amassian, W. Zhang, H. Lu, L. Liu, *et al.*, Hybrid magnonics in hybrid perovskite antiferromagnets, Nat. Commun. **14**, 1834 (2023).

[25] C. Dai and F. Ma, Strong magnon–magnon coupling in synthetic antiferromagnets, Appl. Phys. Lett. **118**, 112405 (2021).

[26] W. He, Z. K. Xie, R. Sun, M. Yang, Y. Li, X.-T. Zhao, W. Liu, Z. D. Zhang, J.-W. Cai, Z.-H. Cheng, *et al.*, Anisotropic magnon–magnon coupling in synthetic antiferromagnets, Chin. Phys. Lett. **38**, 057502 (2021).

[27] M. Li, J. Lu, and W. He, Symmetry breaking induced magnon-magnon coupling in synthetic antiferromagnets, Phys. Rev. B **103**, 064429 (2021).

[28] A. Sud, K. Yamamoto, K. Z. Suzuki, S. Mizukami, and H. Kurebayashi, Magnon-magnon coupling in synthetic ferrimagnets, Phys. Rev. B **108**, 104407 (2023).

[29] X. M. Liu, H. T. Nguyen, J. Ding, M. G. Cottam, and A. O. Adeyeye, Interlayer coupling in $Ni_{80}Fe_{20}/Ru/Ni_{80}Fe_{20}$ multilayer films: Ferromagnetic resonance experiments and theory, Phys. Rev. B **90**, 064428 (2014).

[30] X. Xiao, Z. Chen, C. Dai, and F. Ma, Magnon mode transition in synthetic antiferromagnets induced by perpendicular magnetic anisotropy, J. Appl. Phys. **131**, 093905 (2022).

[31] L. Liensberger, A. Kamra, H. Maier-Flaig, S. Geprägs, A. Erb, S. T. B. Goennenwein, R. Gross, W. Belzig, H. Huebl, and M. Weiler, Exchange-enhanced ultrastrong magnon-magnon coupling in a compensated ferrimagnet, Phys. Rev. Lett. **123**, 117204 (2019).

[32] Y. Wang, Y. Zhang, C. Li, J. Wei, B. He, H. Xu, J. Xia, X. Luo, J. Li, J. Dong, *et al.*, Ultrastrong to nearly deep-strong magnon-magnon coupling with a high degree of freedom in synthetic antiferromagnets, Nat. Commun. **15**, 2077 (2024).

[33] M. Mani Subedi, K. Deng, Y. Xiong, J. Mongeon, M. Tomal Hossain, P. Meisenheimer, E. Zhou, J. Heron, M. B. Jungfleisch, W. Zhang *et al.*, Magnon-magnon interactions induced by spin pumping-driven symmetry breaking in synthetic antiferromagnets, arXiv e-prints, arXiv:2301.07311 (2023).

[34] Y. Wang, D. Zhu, Y. Yang, K. Lee, R. Mishra, G. Go, S.-H. Oh, D.-H. Kim, K. Cai, E. Liu, *et al.*, Magnetization switching by magnon-mediated spin torque through an antiferromagnetic insulator, Science **366**, 1125 (2019).

[35] C. O. Avci, E. Rosenberg, M. Huang, J. Bauer, C. A. Ross, and G. S. D. Beach, Nonlocal detection of out-of-plane magnetization in a magnetic insulator by thermal spin drag, Phys. Rev. Lett. **124**, 027701 (2020).

[36] D. Hayashi, Y. Shiota, M. Ishibashi, R. Hisatomi, T. Moriyama, and T. Ono, Observation of mode splitting by magnon–magnon coupling in synthetic antiferromagnets, Appl. Phys. Express **16**, 053004 (2023).

[37] H. Liu, D. Sun, C. Zhang, M. Groesbeck, R. Mclaughlin, and Z. V. Vardeny, Observation of exceptional points in magnonic parity-time symmetry devices, Sci. Adv. **5**, eaax9144 (2019).

[38] T. Yu, J. Zou, B. Zeng, J. W. Rao, and K. Xia, Non-Hermitian Topological Magnonics, arXiv e-prints, arXiv:2306.04348 (2023).

[39] L. Sheng, M. Elyasi, J. Chen, W. He, Y. Wang, H. Wang, H. Feng, Y. Zhang, I. Medlej, S. Liu, *et al.*, Nonlocal detection of interlayer three-magnon coupling, Phys. Rev. Lett. **130**, 046701 (2023).

[40] O. Lee, K. Yamamoto, M. Umeda, C. W. Zollitsch, M. Elyasi, T. Kikkawa, E. Saitoh, G. E. W. Bauer, and H. Kurebayashi, Nonlinear magnon polaritons, Phys. Rev. Lett. **130**, 046703 (2023).

[41] Z. Wang, M. Gibertini, D. Dumcenco, T. Taniguchi, K. Watanabe, E. Giannini, and A. F. Morpurgo, Determining the phase diagram of atomically thin layered antiferromagnet $CrCl_3$, Nat. Nanotechnol. **14**, 1116 (2019).

[42] S. Yang, X. Xu, Y. Zhu, R. Niu, C. Xu, Y. Peng, X. Cheng, X. Jia, Y. Huang, X. Xu, *et al.*, Odd-even layer-number effect and layer-dependent magnetic phase diagrams in $MnBi_2Te_4$, Phys. Rev. X **11**, 011003 (2021).

[43] Z. Zhang, L. Zhou, P. E. Wigen, and K. Ounadjela, Using ferromagnetic resonance as a sensitive method to study temperature dependence of interlayer exchange coupling, Phys. Rev. Lett. **73**, 336 (1994).

[44] B. Nikin, B. S. Tosic, and V. M. Zekovic, *Introduction to an Analysis of Ferromagnets with Dipole-Dipole Interactions* (De Gruyter, Berlin, Boston, 1974), pp. 449.

[45] C. M. Wynn, M. A. Gîrtu, W. B. Brinckerhoff, K. I. Sugiura, J. S. Miller, and A. J. Epstein, Magnetic dipole−dipole interactions and single-ion anisotropy: Revisiting a classical approach to magnets, Chem. Mater. **9**, 2156 (1997).

[46] J. Sklenar and W. Zhang, Self-hybridization and tunable magnon-magnon coupling in van der Waals synthetic magnets, Phys. Rev. Appl. **15**, 044008 (2021).

[47] S. M. Rezende, C. Chesman, M. A. Lucena, A. Azevedo, F. M. de Aguiar, and S. S. P. Parkin, Studies of coupled metallic magnetic thin-film trilayers, J. Appl. Phys. **84**, 958 (1998).

[48] X. Chen, C. Zheng, S. Zhou, Y. Liu, and Z. Zhang, Ferromagnetic resonance modes of a synthetic antiferromagnet at low magnetic fields, J. Phys.: Condens. Matter **34**, 015802 (2021).

[49] S. Li, Q. Li, J. Xu, S. Yan, G. X. Miao, S. Kang, Y. Dai, J. Jiao, and Y. Lü, Tunable optical mode ferromagnetic resonance in FeCoB/Ru/FeCoB synthetic antiferromagnetic trilayers under uniaxial magnetic anisotropy, Adv. Funct. Mater. **26**, 3738 (2016).

[50] See Supplemental Material http://link.aps.org/supplemental/10.1103/PhysRevApplied.21.054050 for details on magnetization precession trajectories in different modes and unguided experimental resonance spectra.

[51] B. Kuanr, R. E. Camley, and Z. Celinski, Narrowing of the frequency-linewidth in structured magnetic strips: Experiment and theory, Appl. Phys. Lett. **87**, 012502 (2005).

[52] A. Frisk Kockum, A. Miranowicz, S. De Liberato, S. Savasta, and F. Nori, Ultrastrong coupling between light and matter, Nat. Rev. Phys. **1**, 19 (2019).

[53] P. Forn-Díaz, L. Lamata, E. Rico, J. Kono, and E. Solano, Ultrastrong coupling regimes of light-matter interaction, Rev. Mod. Phys. **91**, 025005 (2019).